QUANTUM RESERVOIR COMPUTING FOR EFFICIENT SIGNAL PROCESSING

Project Deliverable

D1.1 Quantitative model of superconducting QR

Lead Beneficiary:	Loughborough University
Author(s):	Gerard McCaul
Contributor(s):	Patrick Navez, Juan Sebastian Totero Gongora, Alex Zagoskin, Aidar Sultanov, Evgeni Ili'ichev
Dissemination Level:	Public (PU)

https://www.qrc-4-esp.eu

Funded by
the European Union

QRC-4-ESP

Document History:

Version and date	Changes
1.0 - 25/10/2024	Initial version

Contents

1 Introduction

In this report we outline the development for the mathematical description of a quantum reservoir (QR) structure comprising several superconducting quantum bits. In Sec. 2 we outline the fabricated transmon system under consideration, and a phenomenological model which captures qualitative behaviour observed in the fabricated transmon system. This model is then refined and fitted to experimental data. This then specifies model parameters required to make quantitative predictions of the fabricated system's behaviour. Sec. 3 assesses the computational capacity of the transmonic system theoretically by developing and testing a framework for reservoir computing. This framework is then applied to experimental data in Sec. 4, in which a benchmark time-series prediction task is successfully performed. Finally, we summarise the results of this deliverable in Sec. 5, and outline the ongoing research questions that will be pursued to further develop the results presented here.

2 Model

2.1 Experimental setup

The system under consideration consists of five transmon qubits, coupled to a coplanar waveguide waveguide resonator. A schematic rendering of this setup is shown in Fig. 1. In the present experiment, each qubit's frequency is controlled via a DC current bias. Using an input microwave signal, the system's transmission coefficient S_{21} can be measured. Full details of the experimental realisation of this system are detailed in [1].

It is possible to capture the qualitative behaviour of this system with a simple phenomenological model, described by:

$$\hat{H} = \sum_{j=1}^{N} \left[\frac{1}{2}\varepsilon_j \hat{\sigma}_j^x + \hat{\sigma}_j^z (\hat{a} + \hat{a}^\dagger) \right] + \omega_c \hat{a}^\dagger \hat{a}. \tag{1}$$

Here $\hat{\sigma}_j^{x,y,z}$ are the usual Pauli matrices describing the jth qubit, with each possessing a Rabi frequency ε_j. The resonator is described by a single mode oscillator with destruction operator $\hat{a}$ and frequency ω_c. In the experiment, each qubit's Rabi frequency can be altered by coupling it to a DC line and applying a bias Φ_0. The effect of this can be observed in the dependence of the measured resonance frequency on this bias. This is illustrated in Fig. 2, which shows both the experimentally observed resonance frequency with bias, and a typical example of the qualitatively similar result predicted by the phenomonological model.

2.2 Theoretical model

In order to make more quantitative predictions of the system's behaviour, we must make some refinements to the model presented above. Specifically, we wish to understand how the qubit Rabi frequencies affect the observed transmission spectrum S_{21}. Beginning from a first-principles model of the system [2], after restricting the resonator to a single photonic mode and applying the rotating wave approximation, we

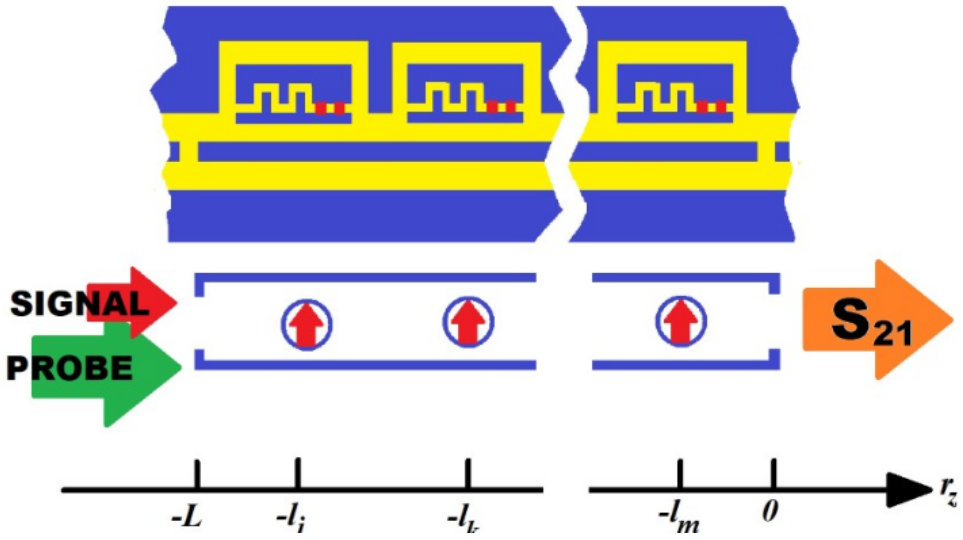

Figure 1: **Upper panel**: Artistic rendering of the fabricated of transmon qubits. Yellow corresponds to insulator region, blue shows the superconducting region, while crosses indicate the position of the Josephson junctions. **Lower panel**: Schematic representation of the QED circuit associated with the device depicted in the upper panel. The blue box with open edges is a cavity resonator, and ovals with vertical arrow are the qubits. The horizontal arrows represent the input signal, probe field and measured transmission S_{21}. The axis is used to indicate the positions l_j of the jth transmon along the r_z direction (the origin is placed after the device as the usual convention in transmission line theory).

obtain the following Hamiltonian:

$$\hat{H} = \sum_{j=1}^{N} -\frac{\sqrt{\varepsilon^2+\Delta_j^2}}{2}\hat{\sigma}_j^z + \frac{g_j}{\sqrt{\varepsilon^2+\Delta_j^2}}[\varepsilon\hat{\sigma}_j^z(\hat{a}+\hat{a}^\dagger) - \Delta_j(\hat{\sigma}_j^-\hat{a}^\dagger + \hat{\sigma}_j^+\hat{a})] + (\delta\omega - i\gamma_c/2)\hat{a}^\dagger\hat{a}. \quad (2)$$

In this model each qubit is presumed to share an identical Rabi frequency ε, with an eigenfrequency ω_j, while the parameters $\Delta_j = \omega_j - \omega_0$ and $\delta\omega = \omega_c - \omega_0$ are defined in relation to the input signal frequency ω_0. The coupling of each qubit to the resonator cavity is described by g_j, while the cavity leakage rate is given by γ_c.

Perturbatively expanding this Hamiltonian up to second order in the coupling parameters, the (complex) eigenfrequency for the photon energy inside the cavity becomes:

$$\omega - i\Gamma/2 = \omega_c - i\gamma_c/2 + \sum_{j=1}^{N} \frac{g_j^2}{\varepsilon^2+\Delta_j^2} \frac{\Delta_j^2}{\sqrt{\varepsilon^2+\Delta_j^2} + \delta\omega - i\gamma_c/2} \quad (3)$$

Physically, the shift in the frequency spectrum results from a virtual photon exciting a qubit. For weak signal ($\varepsilon \to 0$) and for high quality factor ($\gamma_c \ll \Delta_j$), we obtain the expression:

$$\omega = \omega_c + \sum_{j=1}^{N} \frac{g_j^2}{\omega_c - \omega_j}. \quad (4)$$

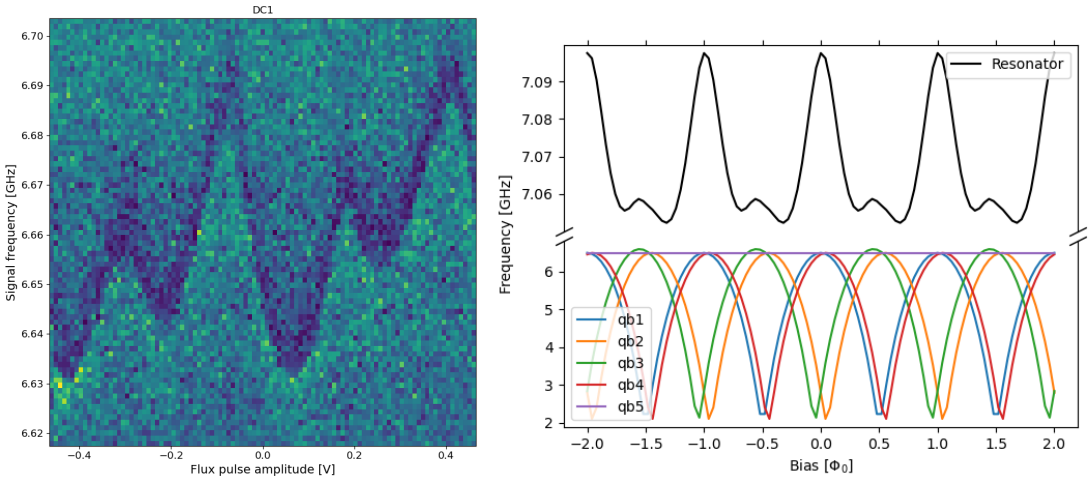

Figure 2: Left panel shows the single tone spectrum for the resonator as the bias on a single qubit is varied. The right panel shows that the phenomenological model's frequency dependence for both the qubits and the single photon resonance. The qualitative behaviour of the latter can be seen to match the former.

The right hand side contains the sum of the half Stark shift associated to each qubit, which corresponds to the frequency shift between the high and low power limit. Assuming equal couplings $g_j = g$, the external power $P = \hbar\omega_c\gamma_c(\varepsilon_0/2g)^2$ is related to the Rabi frequency through the Fabry-Perot-like transmittance relation associated to the resonator:

$$\varepsilon^2 = \frac{\varepsilon_0^2}{1+[(\omega_0-\omega)/(\gamma_c/2)]^2} \tag{5}$$

Eqs. (3) and (5) then form a self consistent set of equations for $\omega(\varepsilon)$. The nonlinear dependency of the power on its frequency in Eq.(5) admits many possible solutions. Consequently we expect the relation between the power and the frequency given a particular value for the Rabi frequency to exhibit some form of bistability.

2.3 Comparison with experimental data

Using this model, it is possible to extract quantitative estimations of system parameters. As an example, the experimental curve shown in Fig. 3 displays a jump reminiscent of the theoretical model's bistability characteristics. If we neglect the dispersion of the qubit frequencies, it is possible to obtain a reasonable fit with experimental data. Fig. 3 shows just such a fit with the experimental curve. To obtain this, we assume identical detuning for the $N = 5$ qubits, together cavity and signal frequencies $\omega_c = \omega_0 = 2\pi \times 6.6102\,GHz$, a half Stark shift of $\omega|_{\varepsilon=0} - \omega_c = 2\pi \times 9.25\,MHz$, and the experimentally determined cavity leakage rate $\gamma_c = 2\pi \times 1.73MHz$ (quality factor $Q = \omega_c/\gamma_c = 3820$). With these parameters obtain a good quantitative agreement between theoretical calculations and the experimental data.

Such a fit however predicts values for the detuning roughly an order of magnitude too large to be realised $\Delta_j = 2\pi \times 7.77\,GHz$, and a coupling $g = 2\pi \times 120\,MHz$. Adjusting the power to the cavity by 10 dBm, more reasonable values are obtained both for detuning $\Delta_j = 2\pi \times 0.78\,GHz$ and the coupling $g = 2\pi \times 38\,MHz$.

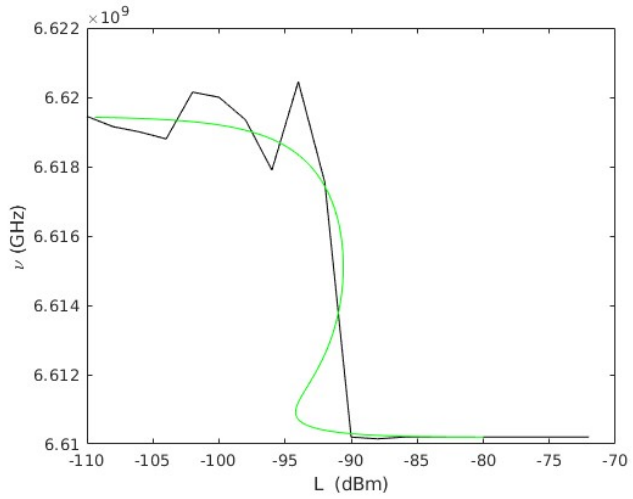

Figure 3: Dependance of the resonant frequency to input power, defining L as power in dBm units (i.e., $P = 1\ \text{mW} \cdot 10^{L/10}$). The fit obtained from the theoretical model is drawn in green with experimental data in black.

3 Reservoir Computing Framework

3.1 Model

Having outlined the experimental setup and the theoretical model describing it, we now turn our attention to the question of how it can be best employed as a reservoir computer. In order to assess the general characteristics required of a physical system to act as a reservoir, we initially model our transmon system using a generic spin model with Markovian dissipation (described via the Lindblad equation). While this projection to the idealised two-level subspace will not capture all dynamics [3–5] - particularly when undergoing fast decay from strong bath coupling [6] - it is instructive to begin here to asses the minimal dynamical complexity necessary for a system to serve as a reservoir. Indeed, the precise dynamics of the reservoir are irrelevant, provided that it possesses the essential prerequisites of non-linearity, fading memory and seperability of processed inputs. In this regard, developing and assessing a pipeline for data processing is best facilitated with a minimal reservoir model, under the expectation that the more sophisticated models describing transmon behaviour specifically can be substituted into the framework as required. Such an incremental approach also allows for the identification of the dynamical properties which lead to an increase in computational capacity as they are incorporated.

Under this scheme, we encode our input time-series data $u(t)$ into the parameters of the Hamiltonian. This naturally maps to the controllable Rabi frequencies of the transmon system outlined in Sec. 2, and avoids the complications of trying to encode data directly into an inherently delicate quantum state. Furthermore, by encoding data directly into the Hamiltonian, we guarantee that any expectations used for linear regression will be a nonlinear function of the input data, even if it is encoded *linearly* into the Hamiltonian parameters.

As an initial model Hamiltonian, we employ system of coupled qubits that has previously been shown to exhibit suitably chaotic behaviour in its [7] dynamics, with the expectation that these will satisfy the essential properties required of the reservoir.

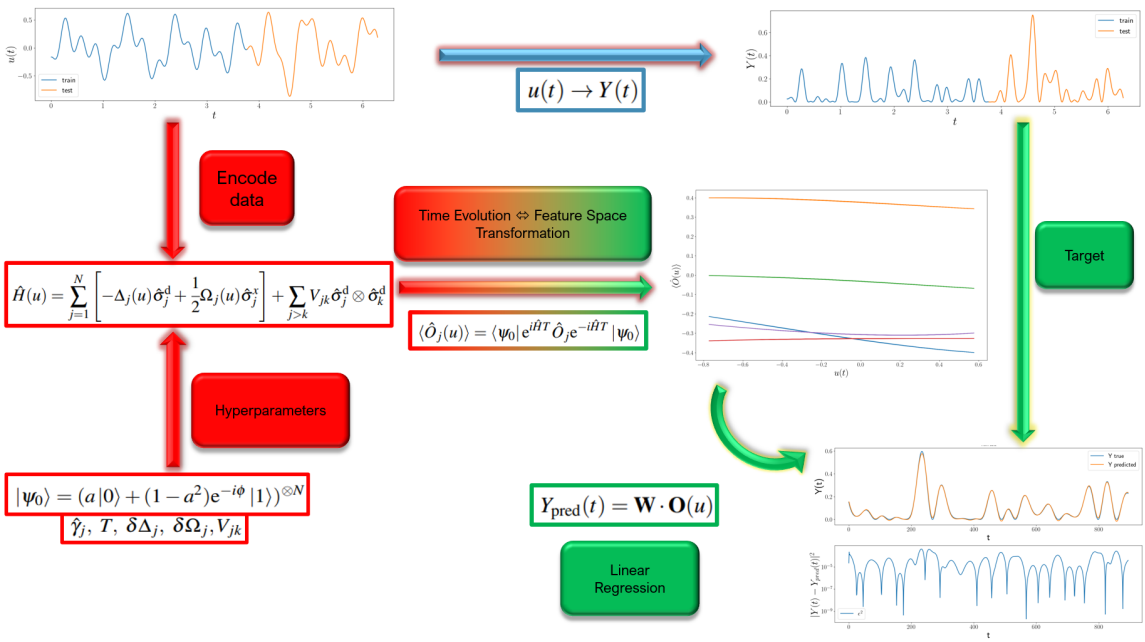

Figure 4: Pipeline for reservoir computing. A datum u is encoded into the quantum system via its Hamiltonian parameters, while other physical parameters of the model serve as effective hyperparameters in the reservoir model. The expectations of the system after time-evolution the act as a feature space transformation of the data, such that these expectations can be used in combination with linear regression to predict a target time-series $Y(t)$.

This can also be thought of as an idealisation of the transmon system in which individual qubits are restricted to a two-level subspace. The Hamiltonian itself consists of N qubits described by:

$$\hat{H}(u) = \sum_{j=1}^{N}\left[-\Delta_j(u)\hat{\sigma}_j^{\mathrm{d}} + \frac{1}{2}\Omega_j(u)\hat{\sigma}_j^{x}\right] + \sum_{j>k} V_{jk}\hat{\sigma}_j^{\mathrm{d}} \otimes \hat{\sigma}_k^{\mathrm{d}} \tag{6}$$

where $\hat{\sigma}_j^{\mathrm{d}}$ is defined in relation to the usual Pauli operators by $\hat{\sigma}_j^{\mathrm{d}} = \frac{1}{2}\left(\hat{1} - \hat{\sigma}_j^{z}\right)$. The datum u is encoded via the single-qubit parameters $\Delta_j(u)$ and $\Omega_j(u)$. In particular, we consider an encoding scheme where the data in encoded as a linear biasing around some central value. That is (for example),

$$\Delta_j(u) = \Delta_0 + \delta\Delta_j + u \tag{7}$$

where Δ_0 is a central value common to each qubit, $\delta\Delta_j$ is a random (but fixed) deviation from this drawn from a normal distribution, to which the appropriately scaled datum is added.

To incorporate dissipation we evolve with a Lindblad master equation, such that the system density dynamics $\hat{\rho}$ are described by

$$\frac{\mathrm{d}}{\mathrm{d}t}\hat{\rho} = -i[\hat{H}, \hat{\rho}] + \mathscr{L}[\hat{\rho}] \tag{8}$$

where the dissipator $\mathscr{L}$ is composed from $\hat{\sigma}_j^{\pm} = \frac{1}{2}(\hat{\sigma}_j^{x} \pm i\hat{\sigma}_j^{y})$, using:

$$\mathscr{L}[\hat{\rho}] = \sum_j \gamma_j \left(\hat{\sigma}_j^{+}\hat{\rho}\hat{\sigma}_j^{-} - \frac{1}{2}\left\{\hat{\sigma}_j^{-}\hat{\sigma}_j^{+}, \hat{\rho}\right\}\right), \tag{9}$$

where γ_j is the strength of dissipative coupling for each qubit. The final physical element of the model, where each qubit is initialised in a state with random parameters for its probability amplitude a_j and relative phase ϕ_j:

$$|\psi_0\rangle = \bigotimes_j^N a_j |0\rangle + (1 - a_j^2) \mathrm{e}^{-i\phi_j} |1\rangle \tag{10}$$

$$\langle \hat{O}_j(u) \rangle = \langle \psi_0 | \, \mathrm{e}^{i\hat{H}T} \hat{O}_j \mathrm{e}^{-i\hat{H}T} \, | \psi_0 \rangle \tag{11}$$

The reservoir computing for this system is then as follows. The Hamiltonian encodes data into the quantum system, which is transferred to the state via evolution for some time T. This is then read out from the expectations of a set of observable operators $\hat{O}_j$, given by:

$$\langle \hat{O}_j(u) \rangle = \langle \psi_0 | \, \mathrm{e}^{i\hat{H}T} \hat{O}_j \mathrm{e}^{-i\hat{H}T} \, | \psi_0 \rangle \, . \tag{12}$$

These expectations represent a feature space transformation of the initial data, and are used for training a linear regression model. In the present case we consider one dimensional time-series, where the input data $u(t)$ are used to predict some target series $Y(t)$. Using ridge regression, a set of weights $\mathbf{W}$, are then calculated to produce the best fit to the target Y, with the reservoir prediction being given by

$$Y_{\mathrm{pred}}(t) = \mathbf{W} \cdot \mathbf{O}(u(t)). \tag{13}$$

The model's predictive capacity is then tested by using Eq. (13) with the learned weights $\mathbf{W}$ for data not included in the original training set. The full pipeline for this process is schematically illustrated in Fig. 4, with the codebase used for its simulation available at [8].

3.2 Model results

In order to test the degree to which this low-dimensional approximation to transmonic systems is able to perform prediction, we consider three distinct tasks performed on a variety of datasets. These tasks are:

- **Function synthesis**: the target outcome time-series is some function of the input time, series. i.e. if we have an input-time series $u(t)$ then synthesis sets the target $y(t_k) = f(u(t_k))$, where f is some (non-linear) function.
- **Non-autonomous prediction**: Here the outcome time-series target is to predict the next value in the input series - $y(t_k) = u(t_{k-1})$.
- **Autonomous prediction**: As above, but in this case the target prediction for $y(t_k)$ is then used as the input for the next point in the target series, $y(t_{k+1})$.

Critically, any of the regression tasks with the benchmark datasets can only be achieved with a nonlinear transformation of the input time-series. In this regard, they serve as a check on the presence of the vital prerequisites for any reservoir - namely nonlinear transformation of data and separability of that data in readout outcomes. Examples of these three tasks using a random sum of sine waves are highlighted in Fig. 5.

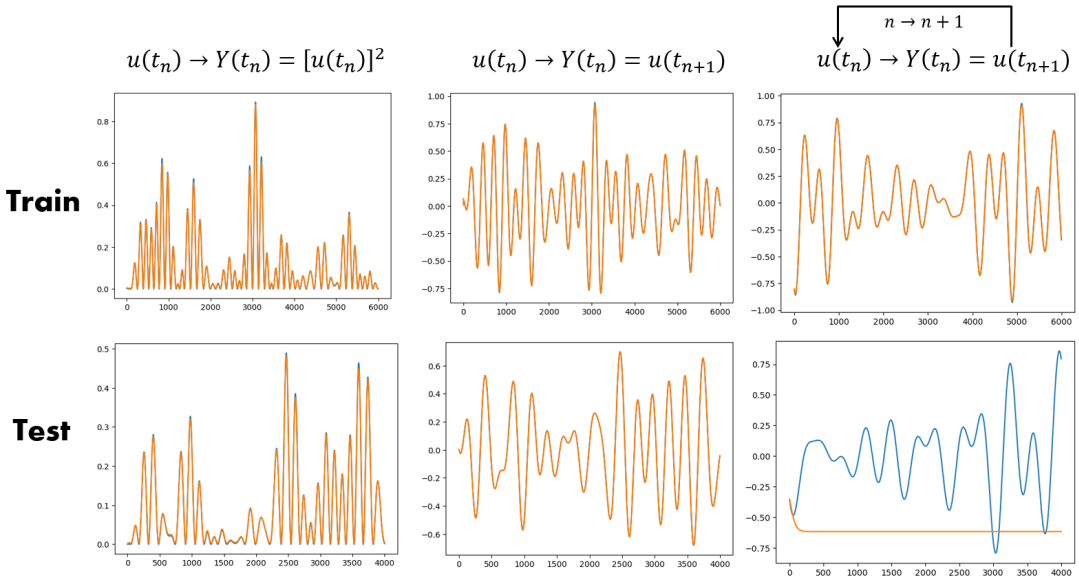

Figure 5: The three categories of prediction task, using the example of a sum of random sine-waves. Each example plot includes both the target data (blue) and reservoir predict (orange). In both the synthesis and non-autonomous prediction the reservoir is able to obtain excellent accuracy. For autonomous prediction the absence of memory in the simple encoding scheme leads to autonomous prediction testing predictions rapidly failing.

For both synthesis and non-autonomous prediction, we find that excellent performance is acheived over a wide parameter range, with the chief determinant of both training and testing accuracy being the number of qubits employed. The effective reservoir model is highly tunable, with a large number of effective hyperparameters that will impact dynamics. This includes the evolution time T, the strength of the environmental damping γ, the distribution of Hamiltonian parameters (outside of those directly dependent on u), as well as the initial state parameterisation). Notably, we find that learning performance is in many cases largely insensitive to the the hyperparameter values over a reasonably large range. As might be expected however, this insensitivity is task dependent. For the prediction of Mackey glasses, the reservoir achieves similar performace even in the absence of interaction, while the random sinusoid task shows marked improvement when interactions are included. The global exception to any hyperparameter insensitivity is for extreme damping, which when combined with a sufficiently long evolution tends the system to a steady state only very weakly dependent on the encoded data. In such a scenario performance is severely degraded. This is in some sense an indication that the manner in which the reservoir processes information (in this encoding scheme) is intrinsically quantum, given the fact that sufficiently strong decoherence will render that information unrecoverable.

One weakness of the current approach is that autonomous predictions quickly diverge from their target in testing. This is indicative of a lack of memory in this simple protocol. This is a natural consequence of a framework in which each datum is processed in a separate, re-initialised evolution. Consequently the system only contains information of the local point in the time-series it is processing, while autonomous prediction benefits from some fading memory of previous points in the time-series.

4 Transmonic Reservoir Computing

Taken together, the results detailed in the previous sections imply that the fabricated transmon system is already capable of performing simple reservoir calculations. This is due to the fact that the even the simple phenomological model defined in Sec. 2 is able to qualitatively capture the observed experimental input (current bias) - output (photon resonance frequency) relationship, and is of a functionally equivalent complexity to the model Hamiltonian used to perform calculations in Sec. 3. Consequently, there is a reasonable expectation that by encoding data directly into the bias current of the qubits, and using the resonance frequency as the readout variable, computations can be implemented.

To demonstrate this, for each of the four qubits we extract the photon resonance response curve from the collected spectral data shown in Fig. 6. By mapping computation input data onto the domain of the bias current, these curves may then serve as the feature space transformations illustrated in Fig 4. An example calculation directly employing this methodology is present in Fig. 7, where it is used to perform non-autonomous prediction of a Mackey glass. In both training and testing, it is possible to achieve excellent accuracy, providing a proof-of-principle demonstration of transmonic reservoir computing.

5 Outlook

Starting from a universal model for qubits, we have constructed a framework in which their capacity to act as a reservoir computer has been confirmed using a set of time-series analysis benchmarks. We have found that with slight modification this model is able to capture the essential features observed in a fabricated transmonic system. Consequently, it has been possible to directly incorporate experimental data into the reservoir framework to successfully perform calculations.

Having established this base, we foresee a number of opportunities to further improve upon the results presented here. In terms of physical implementation, we expect to employ experimental data to further refine the numerical models employed in the computing framework. For example, the single tone spectra observed in experiments can - after curve extraction and fitting, be used as a target for finding the optimal physical model parameters which most closely align the numerical model's observable prediction to those of the experiment. Testing computational performance in this model will then inform the optimal experimental regime for performing reservoir calculations.

More generally, the present numerical models may benefit from a more sophisticated treatment of environmental interactions. At present the Lindbladian dissipators use to model this presume a Markovian character to dynamics, while more sophisticated more sophisticated techniques such as the stochastic Liouville von-Neumann equation [6, 9] endow the physical dynamics with memory. This feature not only is required to more accurately match experimental observation, but also represents a potential computing resource that must be properly modeled to be exploited. A related point is the failure of the autonomous prediction task in this setup, as it requires some memory in the system linking processed data points.

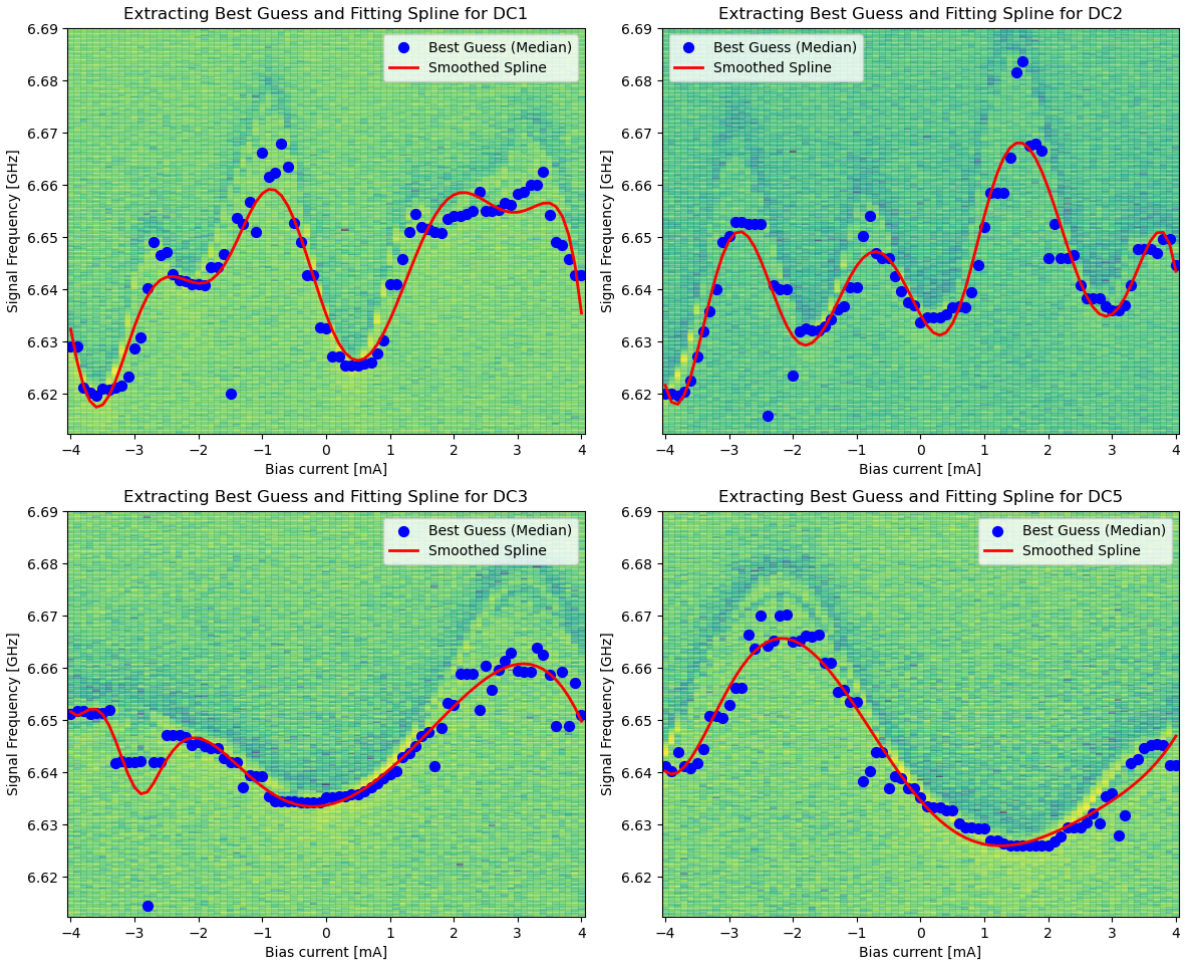

Figure 6: Extracting the photon resonance frequency from spectral data. First a median filter is applied, from which a 'best guess' for the resonance frequency at each current value is extracted. A response curve is then fitted from these points, to be employed as a feature space transformation for the computation.

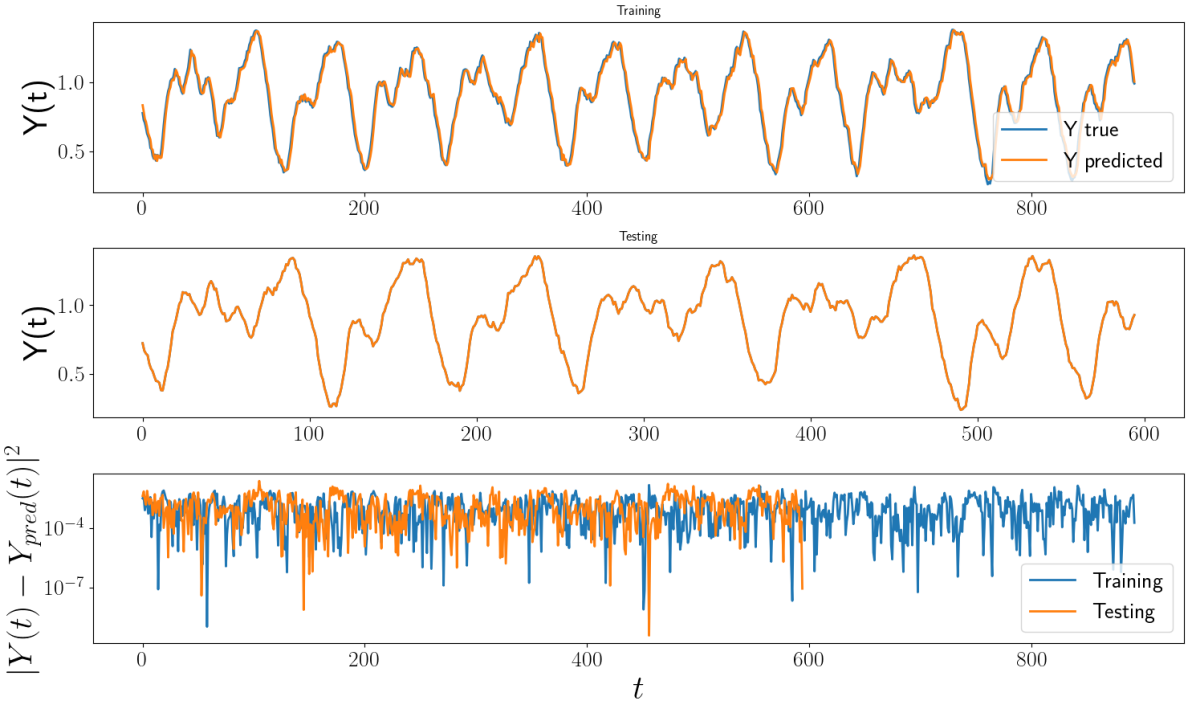

Figure 7: Mackey glass non-autonomous prediction task, using the single photon resonance frequency as the readout variable.

References

[1] E. Mutsenik, A. Sultanov, S. Linzen, M. Schmelz, D. Kalacheva, O. Astafiev, G. Oelsner, M. Ziegler, U. Hübner, R. Stolz, and E. Il'ichev. Controllable coupling between fundamental modes in an asymmetric superconducting coplanar waveguide resonator. Applied Physics Letters, 125(4):042601, July 2024.

[2] P. Navez, A. G. Balanov, S. E. Savel'ev, and A. M. Zagoskin. Quantum electrodynamics of non-demolition detection of single microwave photon by superconducting qubit array. Journal of Applied Physics, 133(10):104401, March 2023.

[3] N G Dickson, M W Johnson, M H Amin, R Harris, F Altomare, A J Berkley, P Bunyk, J Cai, E M Chapple, P Chavez, F Cioata, T Cirip, P deBuen, M Drew-Brook, C Enderud, S Gildert, F Hamze, J P Hilton, E Hoskinson, K Karimi, E Ladizinsky, N Ladizinsky, T Lanting, T Mahon, R Neufeld, T Oh, I Perminov, C Petroff, A Przybysz, C Rich, P Spear, A Tcaciuc, M C Thom, E Tolkacheva, S Uchaikin, J Wang, A B Wilson, Z Merali, and G Rose. Thermally assisted quantum annealing of a 16-qubit problem. Nature Communications, 4(1):1903, May 2013.

[4] M. W. Johnson, M. H. S. Amin, S. Gildert, T. Lanting, F. Hamze, N. Dickson, R. Harris, A. J. Berkley, J. Johansson, P. Bunyk, E. M. Chapple, C. Enderud, J. P. Hilton, K. Karimi, E. Ladizinsky, N. Ladizinsky, T. Oh, I. Perminov, C. Rich, M. C. Thom, E. Tolkacheva, C. J. S. Truncik, S. Uchaikin, J. Wang, B. Wilson, and G. Rose. Quantum annealing with manufactured spins. Nature, 473(7346):194–198, May 2011.

[5] Sergio Boixo, Troels F. Rønnow, Sergei V. Isakov, Zhihui Wang, David Wecker,

Daniel A. Lidar, John M. Martinis, and Matthias Troyer. Evidence for quantum annealing with more than one hundred qubits. Nature Physics, 10(3):218–224, March 2014.

[6] Aravind Plathanam Babu, Jani Tuorila, and Tapio Ala-Nissila. State leakage during fast decay and control of a superconducting transmon qubit. npj Quantum Information, 7(1):1–8, February 2021. Publisher: Nature Publishing Group.

[7] A. V. Andreev, A. G. Balanov, T. M. Fromhold, M. T. Greenaway, A. E. Hramov, W. Li, V. V. Makarov, and A. M. Zagoskin. Emergence and control of complex behaviors in driven systems of interacting qubits with dissipation. npj Quantum Information, 7(1):1, January 2021.

[8] Qrc-4-esp github repository. https://github.com/jstotero/QRC-4-ESP_LU, 2024. Accessed: 2024-10-20.

[9] Jürgen T. Stockburger. Simulating spin-boson dynamics with stochastic Liouville-von Neumann equations. Chem. Phys., 296:159–169, 2004.